



Position observation-based calibration method for an LDV/SINS integrated navigation system

ZHIYI XIANG, QI WANG, RONG HUANG, CHONGBIN XI, XIAOMING NIE, AND JIAN ZHOU*

College of Advanced Interdisciplinary Studies, National University of Defense Technology, Changsha 410073, China

*Corresponding author: wttzhoujian@163.com

Received 6 May 2021; revised 6 August 2021; accepted 8 August 2021; posted 9 August 2021 (Doc. ID 430866); published 2 September 2021

With the advantages of high velocity measurement accuracy and fast dynamic response, the laser Doppler velocimeter (LDV) is expected to replace the odometer to be combined with a strapdown inertial navigation system (SINS) to form a higher precision integrated navigation system. However, LDV scale factor error and misalignment angles between LDV and inertial measurement unit will affect the accuracy of navigation. Considering that not all global navigation satellite system (GNSS) receivers can directly provide velocity information and current mainstream calibration methods are sensitive to the measurement noise and outliers of velocity and position information, a robust calibration method aided by GNSS is proposed in this paper, which is based on position observation. Different from current popular calibration methods, the attitude information of the GNSS/SINS integrated navigation system obtained by an adaptive Kalman filter is used to construct the observation vector together with LDV velocity outputs and GNSS position outputs in this method. The LDV scale factor error and the misalignment angle are determined by the ratio of two observation vector modulus and the Davenport's q-method method, respectively. The accuracy and robustness of the calibration method are verified by one vehicle test with normal GNSS signals and one vehicle test with GNSS signals with outliers. And the horizontal position error of dead reckoning of the calibrated LDV/SINS integrated system are less than 0.0314% and 0.1033% of the mileage, respectively. © 2021 Optical Society of America

<https://doi.org/10.1364/AO.430866>

1. INTRODUCTION

The strapdown inertial navigation system (SINS) is widely used at present on account of its remarkable advantages such as high reliability, strong overload capacity, fast start-up, and so on. Due to the initial alignment error and inertial sensors errors, the positioning errors of the SINS will accumulate along with time. Therefore, integrated navigation has become the mainstream direction of development at present [1–3].

A global navigation satellite system (GNSS) can provide accurate velocity and position information to correct the cumulative error of the SINS and restrain the divergence of positioning error of the navigation system [4]. Therefore, a GNSS/SINS integrated navigation system is widely used in the positioning of land vehicles and surface ships. However, the GNSS is not always reliable in complex environments, such as tunnels, wooded areas, and urban canyons. Sensors such as odometers (ODs), Doppler velocity logs (DVL), and SINSs do not rely on external signals, thus the OD/SINS and DVL/SINS integrated navigation systems can resist the interference of the surrounding environment [5–8]. However, the measurement result of OD relates to the wheel circumference and the rotation angle, and the vehicle driving state and tire state will greatly affect the measurement accuracy [9]. Based on the acoustic Doppler effect,

the DVL has weaknesses such as poor accuracy and real-time performance of velocity measurement since the acoustic signal is easy to be disturbed and the propagation speed of the acoustic wave is not fast enough.

Based on the laser Doppler effect, the laser Doppler velocimeter (LDV) has the advantages of high accuracy, rapid dynamic response, non-contact measurement, good directional sensitivity, complete autonomy, and good spatial resolution [10]. Thus, the LDV has obtained extensive use including in biomedicine, meteorological observation, fluid flow velocity measurement, and so on. In recent years, our research group has proposed and developed a variety of LDVs with reference-beam structure to measure true vehicle velocity over ground. Therefore, the LDV can be integrated with the SINS to construct an LDV/SINS integrated navigation system for land autonomous navigation field [11–15]. Due to the LDV having high sampling frequency, the LDV/SINS integrated navigation system can be considered to have no time delay in the ideal conditions.

In LDV/SINS integrated navigation systems, the coordinate system of the LDV is hard to coincide with the body frame. And the errors also exist between the actual inclination angle of the LDV beam to the ground and the design value, which will lead to scale factor error. In order to improve the navigation accuracy, the misalignment angles ϕ and scale factor error

δK should be calibrated. For the integrated navigation system composed of a speed sensor and SINS, the calibration methods commonly include the Kalman-based online calibration method [16–18], the track calibration method, and the optimal estimation method based on solving Wahba's problem [19–22]. The online calibration method is an effective method estimating installation error angle and scale factor error by the Kalman filter. However, the observability of the LDV error parameters is related to the navigation trajectory, and it is inconvenient to determine the initial filtering parameters. In addition, the computation of the standard Kalman filtering algorithm is proportional to the cubic power of the state dimension, and the increase of the state dimension makes the calculation amount increase as geometric series. The track calibration method is not conducive to rapid system calibration, because it requires long-term operation on the designated track. There are many optimal estimation methods based on solving Wahba's problem. Compared with the Kalman filter, most optimal estimation methods have less computation and simple implementation, but the estimation performance depends heavily on the accuracy of the established model. At present, the literature about the online calibration scheme of vehicle LDV all adopts the calibration method based on the Kalman filter [23,24].

In this paper, a LDV error calibration method based on position observation is proposed. The attitude information of the GNSS/SINS integrated navigation, GNSS position output, and LDV output are used to establish position observations. For the accuracy of position observations, adaptive filtering is used in the process of GNSS/SINS integrated navigation. The scale factor error of the LDV is determined by the ratio of two observation vector modulus, and the misalignment angle of the LDV is determined by solving two observation vectors by Davenport's q-method [25,26].

The rest of this paper is organized as follows. In Section 2, the principle of the one-dimensional split-reuse reference-beam LDV is introduced. In Section 3, a calibration method based on velocity observation is proposed. In Section 4, a calibration method based on position observation is proposed. In Section 5, the proposed method is compared with the existing typical methods by using the vehicle-mounted field test data collected from LDV-aided laser SINS. Concluding remarks are given in Section 6.

2. PRINCIPLE OF THE ONE-DIMENSIONAL SPLIT-REUSE REFERENCE-BEAM LDV

The optical structure of the one-dimensional split-reuse reference-beam LDV is shown in Fig. 1. The laser source is a Nd : YVO₄ laser operating in single longitudinal mode and the TEM₀₀ transverse mode, with the power of 50 mW and the wavelength of 532 nm. The light passes through the collimation and compression lens and splits into a reflected and a transmitted beam with equal intensity by the beam splitter BS1 with a reflectivity of 50%. The reflected beam is then split into two parts by a beam splitter BS2 with a reflectivity of 98%. The transmitted beam is passed through the attenuator and reflected by the total reflecting mirror M1, called the reference beam. The reflected beam is reflected to the ground by M2 and M3, and the transmitted beam from BS1 is incident on the

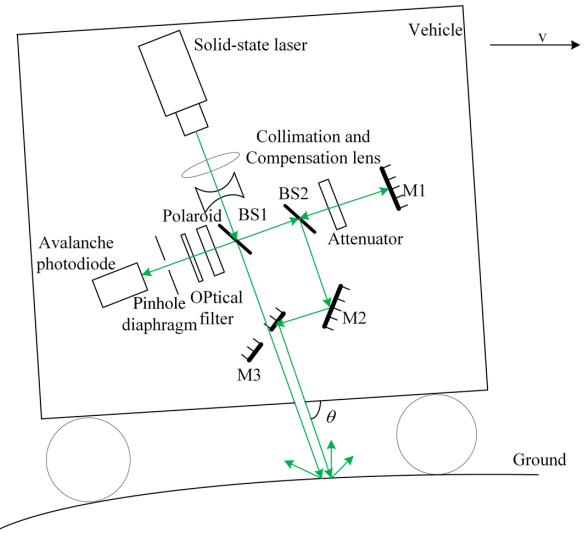


Fig. 1. Optical schematic of the one-dimensional split-reuse reference-beam LDV.

ground in the same direction through the central hole of total reflecting mirror M3. Part of the scattered beam passing through the central hole of M3 is reflected by BS1, and then incident to the avalanche photodiode as the signal beam through the polarizer, optical filter, and pinhole diaphragm. The signal beam and the reference beam interfere on the photosensitive surface of the detector to form a Doppler beat signal. The relationship between the vehicle velocity v_{LDV} output by the LDV and the Doppler frequency f_D is [27]

$$v_{LDV} = \lambda f_D / (2 \cos \theta) = K f_D, \quad (1)$$

where λ is the wavelength of the laser, θ is the inclination angle of the laser beam incident on the ground, and K is the scale factor of the LDV.

3. CALIBRATION METHOD BASED ON VELOCITY OBSERVATION

In this paper, the local level navigation frame is denoted as the n frame, the vehicle body frame is denoted as the b frame, the inertial non-rotating frame is denoted as the i frame, the Earth frame is denoted as the e frame, and the frame in which the LDV is located is denoted as the m frame.

A. GNSS/SINS Integrated Navigation

In order to improve the calibration speed and accuracy, GNSS information is used in the calibration process. Therefore, a loosely couple GNSS/SINS integrated navigation system is designed, and the error model of the SINS is given by [28]

$$\dot{\boldsymbol{\varphi}} = \boldsymbol{\varphi} \times \boldsymbol{\omega}_{in}^n + \delta \boldsymbol{\omega}_{in}^n - \mathbf{C}_b^n \boldsymbol{\varepsilon}_{ib}^b, \quad (2)$$

$$\begin{aligned} \delta \dot{\boldsymbol{v}}^n &= -\boldsymbol{\varphi} \times \boldsymbol{f}^n + \delta \boldsymbol{v}^n \times (2\boldsymbol{\omega}_{ie}^n + \boldsymbol{\omega}_{en}^n) \\ &+ \boldsymbol{v}^n \times (2\delta \boldsymbol{\omega}_{ie}^n + \delta \boldsymbol{\omega}_{en}^n) + \mathbf{C}_b^n \nabla_{ib}^b, \end{aligned} \quad (3)$$

$$\delta \dot{L} = \delta v_N / (R_M + h) - v_N \delta h / (R_M + h)^2, \quad (4)$$

$$\begin{aligned}\dot{\delta\lambda} &= \sec L \delta v_E / (R_N + h) + v_E \tan L \sec L \delta L / (R_N + h) \\ &\quad - v_E \sec L \delta h / (R_N + h)^2, \quad (5) \\ \dot{\delta h} &= \delta v_U, \quad (6)\end{aligned}$$

$$\dot{\boldsymbol{\varepsilon}}_{ib}^b = \mathbf{0}_{3 \times 1}, \quad (7)$$

$$\dot{\nabla}_{ib}^b = \mathbf{0}_{3 \times 1}, \quad (8)$$

where $\boldsymbol{\varphi}$ is the attitude error of SINS, \mathbf{C}_b^n is the attitude matrix from the b frame to the n frame, $\mathbf{v}^n = [v_E \ v_N \ v_U]^T$ is the velocity of SINS, L is latitude, λ is longitude, and h is altitude. $\boldsymbol{\omega}_{in}^n$ is the angular rate of the n frame with respect to the i frame, $\boldsymbol{\omega}_{en}^n$ is the angular rate of the n frame to the e frame, $\boldsymbol{\omega}_{ie}^n$ represents the earth rotation rate in the n frame. R_M and R_N are the principal radius of curvature of the prime meridian and the equator, respectively. \mathbf{f}^n denotes the specific force in the n frame, $\boldsymbol{\varepsilon}_{ib}^b$ denotes the sum of gyro constant bias and white noise vectors, and ∇_{ib}^b denotes the sum of accelerometer constant bias and white noise vectors. $(\cdot) \times$ means to solve the antisymmetric matrix. The 15-dimensionan state of the system model of the Kalman filter is written as

$$\mathbf{X} = \left[\boldsymbol{\varphi}^T \ \delta \mathbf{v}^T \ \delta \mathbf{P}^T \ (\boldsymbol{\varepsilon}_{ib}^b)^T \ (\nabla_{ib}^b)^T \right]^T, \quad (9)$$

where $\delta \mathbf{P} = [\delta L \ \delta \lambda \ \delta h]^T$ denotes position error vectors.

Based on Eqs. (2)–(8), the state equation can be obtained as follows:

$$\dot{\mathbf{X}}_k = \mathbf{F}_k \mathbf{X}_k + \mathbf{G}_k \mathbf{w}_k, \quad (10)$$

where \mathbf{F}_k is the system state transition matrix, \mathbf{G}_k is the noise transfer matrix, and \mathbf{w}_k is the system noise vector.

The velocity and position differences between the GNSS and SINS are chosen as the measurement equation in the GNSS/SINS integrated navigation system. And the measurement equation is

$$\mathbf{z}_k = \begin{bmatrix} \mathbf{v}_{\text{SINS}} - \mathbf{v}_{\text{GNSS}} \\ \mathbf{P}_{\text{SINS}} - \mathbf{P}_{\text{GNSS}} \end{bmatrix} = \mathbf{H}_k \mathbf{X}_k + \mathbf{V}_k, \quad (11)$$

where $\mathbf{H}_k = [\mathbf{0}_{6 \times 3} \ \mathbf{I}_{6 \times 6} \ \mathbf{0}_{6 \times 6}]$, \mathbf{V}_k is the zero-mean Gaussian white noise vector, and $\mathbf{I}_{6 \times 6}$ is the 6×6 identity matrix.

B. Calibration Algorithm

According to Eq. (1), the vehicle velocity output by the LDV in the m frame can be given by

$$\mathbf{v}_{\text{LDV}}^m = [0 \ v_{\text{LDV}} \ 0]^T. \quad (12)$$

Using the velocity and attitude information provided by the GNSS/SINS integrated navigation system, the “true” velocity in the b frame can be obtained as

$$\mathbf{v}^b = \mathbf{C}_n^b \mathbf{v}^n, \quad (13)$$

where \mathbf{v}^n is the velocity under the n frame obtained from the GNSS/SINS integrated navigation system, and \mathbf{C}_n^b is the

direction cosine matrix obtained from the GNSS/SINS integrated navigation system. The output velocity of the LDV in the m frame can be orthogonally decomposed into the b frame as

$$\mathbf{v}^b = \mathbf{C}_m^b \mathbf{v}_{\text{LDV}}^m + \boldsymbol{\omega}_{nb}^b \times \mathbf{l}_{\text{LDV}}^b, \quad (14)$$

$$\mathbf{C}_m^b = \mathbf{I}_{3 \times 3} - \boldsymbol{\phi} \times, \quad (15)$$

where \mathbf{C}_m^b is the coordinate transformation matrix between the b frame and the m frame, $\boldsymbol{\omega}_{nb}^b$ is the angular rate, and $\mathbf{l}_{\text{LDV}}^b$ is the LDV lever arm, which can be measured accurately by total station. It can be seen from [29] that the roll misalignment angle has no effects on the calibration result of the LDV, so $\boldsymbol{\phi}$ can be written as

$$\boldsymbol{\phi} = [\boldsymbol{\phi}_{mx} \ 0 \ \boldsymbol{\phi}_{mz}]^T, \quad (16)$$

where $\boldsymbol{\phi}_{mx}$ is the pitch misalignment angle and $\boldsymbol{\phi}_{mz}$ is the heading misalignment angle.

It is known from Eq. (1) that the scale factor of the LDV is related to the inclination angle of LDV design. Due to the deviation between the actual inclination angle and the design inclination angle of the LDV, it is necessary to compensate the scale factor error. Since the installation position of the LDV is close to the inertial measurement unit, the influence of the lever arm effect is ignored in this paper. Thus Eq. (14) can be rewritten as

$$\mathbf{v}^b = (1 + \delta K) \mathbf{C}_m^b \mathbf{v}_{\text{LDV}}^m, \quad (17)$$

where δK is the LDV scale factor error.

Substituting Eq. (13) into Eq. (17), the observation equation can be expressed as

$$\mathbf{C}_n^b \mathbf{v}^n = (1 + \delta K) \mathbf{C}_m^b \mathbf{v}_{\text{LDV}}^m. \quad (18)$$

Since the attitude matrix does not change the magnitude of the vector, the scale factor error can be calculated as [30]

$$\delta K = \|\mathbf{C}_n^b \mathbf{v}^n\| / \|\mathbf{v}_{\text{LDV}}^m\| - 1, \quad (19)$$

where $\|\cdot\|$ denotes taking the vector modulus.

Define two vectors as

$$\begin{cases} \boldsymbol{\alpha}(k) = (1 + \delta K) \mathbf{v}_{\text{LDV}}^m \\ \boldsymbol{\beta}(k) = \mathbf{C}_n^b \mathbf{v}^n \end{cases}. \quad (20)$$

The observation vector equation can be given by

$$\boldsymbol{\beta}(k) = \mathbf{C}_m^b \boldsymbol{\alpha}(k). \quad (21)$$

Since $\boldsymbol{\alpha}(k)$ and $\boldsymbol{\beta}(k)$ are known vectors, the problem of solving the misalignment angle matrix \mathbf{C}_m^b is equivalent to the problem of continuous attitude determination using vector observations, that is, the Wahba’s problem, and many fruitful algorithms can be readily used [31]. In this paper, the Davenport’s q-method is used estimate the misalignment angle matrix. The misalignment angle matrix \mathbf{C}_m^b can be formulated by its corresponding unit quaternion $\mathbf{q} = [q_0, \boldsymbol{\rho}^T]^T$, where q_0 is the scalar part and the $\boldsymbol{\rho}$ is the vector part, subject to $\mathbf{q}^T \mathbf{q} = 1$. \mathbf{C}_m^b can be expressed as [32]

$$\mathbf{C}_m^b = (q_0^2 - \boldsymbol{\rho}^T \boldsymbol{\rho}) \mathbf{I}_{3 \times 3} + 2\boldsymbol{\rho}\boldsymbol{\rho}^T - 2q_0(\boldsymbol{\rho} \times). \quad (22)$$

The quaternion form of vector observations is as follows:

$$\begin{cases} \boldsymbol{\alpha}_q(k) = [0 \ \boldsymbol{\alpha}(k)^T]^T \\ \boldsymbol{\beta}_q(k) = [0 \ \boldsymbol{\beta}(k)^T]^T \end{cases}. \quad (23)$$

Equation (21) can be rewritten as

$$\boldsymbol{\beta}_q(k) \otimes \boldsymbol{q} = \boldsymbol{q} \otimes \boldsymbol{\alpha}_q(k) \otimes \boldsymbol{q}^*, \quad (24)$$

where \otimes denotes the quaternion multiplication, and the superscript * denotes the conjugate form of the quaternion.

In Eq. (24), multiplying both sides from right by \boldsymbol{q} and rearranging as

$$\boldsymbol{\beta}_q(k) \otimes \boldsymbol{q} - \boldsymbol{q} \otimes \boldsymbol{\alpha}_q(k) = 0. \quad (25)$$

According to the properties of quaternion multiplication, Eq. (25) can be written as

$$\left([\boldsymbol{\beta}_q^+(k)] - [\boldsymbol{\alpha}_q^-(k)] \right) \boldsymbol{q} = 0, \quad (26)$$

where

$$[\boldsymbol{\alpha}_q^-(k)] = \begin{bmatrix} 0 & -\boldsymbol{\alpha}(k)^T \\ \boldsymbol{\alpha}(k) & -\boldsymbol{\alpha}(k) \times \end{bmatrix}, \quad (27)$$

$$[\boldsymbol{\beta}_q^+(k)] = \begin{bmatrix} 0 & -\boldsymbol{\beta}(k)^T \\ \boldsymbol{\beta}(k) & \boldsymbol{\beta}(k) \times \end{bmatrix}. \quad (28)$$

Following the Davenport's q-method, the attitude quaternion can be determined by solving the following optimization problems:

$$J = \min_{\boldsymbol{q}} \boldsymbol{q}^T \boldsymbol{M} \boldsymbol{q}, \quad (29)$$

where

$$\boldsymbol{M} = \int_0^k \left([\boldsymbol{\beta}_q^+(t)] - [\boldsymbol{\alpha}_q^-(t)] \right)^T \left([\boldsymbol{\beta}_q^+(t)] - [\boldsymbol{\alpha}_q^-(t)] \right) dt. \quad (30)$$

Therefore, the attitude determination problem is equivalent to determining the unit quaternion that minimizes Eq. (29). In [33] it is proved that the optimal quaternion is the normalized eigenvector corresponding to the smallest eigenvalue of \boldsymbol{M} , and the smallest eigenvalue is unique.

4. CALIBRATION METHOD BASED ON POSITION OBSERVATION

Currently, the calibration methods based on GNSS velocity information have two major defects. The first defect is that not all GNSS receivers can provide ground velocity, and the accuracy of solving velocity based on GNSS position information will be lost. The second defect is that the outliers contained in the GNSS velocity will degrade the performance of the calibration. Although this defect can be reduced by using the velocity information provided by the GNSS/SINS integrated navigation system, the LDV velocity measurement noise and outliers will also affect the accuracy of calibration. In order to improve the calibration accuracy, the improvements are made to the construction of the observation model in this section.

Due to the inaccurate modeling of measurement noise in the modeling of the GNSS/SINS integrated navigation system, the accuracy of Kalman filtering is reduced, thus the accuracy of velocity and attitude information provided by GNSS/SINS integration is reduced, and finally reduces the calibration accuracy. Therefore, it is necessary to adjust the measurement noise based on the innovation vector.

The innovation vector is

$$\boldsymbol{e}_k = \boldsymbol{z}_k - \boldsymbol{H}_k \hat{\boldsymbol{X}}_k^-, \quad (31)$$

where $\hat{\boldsymbol{X}}_k^-$ is the predicted value of the state vector in the Kalman filter.

By calculating the variance of both sides of Eq. (31), we can get

$$\mathbf{E} [\boldsymbol{e}_k \boldsymbol{e}_k^T] = \boldsymbol{H}_k \boldsymbol{P}_k^- \boldsymbol{H}_k^T + \boldsymbol{R}_k, \quad (32)$$

where \boldsymbol{P}_k^- is the prediction state covariance matrix in the Kalman filter.

According to Eq. (32), the measurement noise covariance matrix \boldsymbol{R}_k is given by

$$\begin{aligned} \boldsymbol{R}_k &= \frac{1}{k} \sum_{i=1}^k (\boldsymbol{e}_i \boldsymbol{e}_i^T - \boldsymbol{H}_i \boldsymbol{P}_i^- \boldsymbol{H}_i^T) \\ &= \frac{1}{k} \left[\sum_{i=1}^{k-1} (\boldsymbol{e}_i \boldsymbol{e}_i^T - \boldsymbol{H}_i \boldsymbol{P}_i^- \boldsymbol{H}_i^T) \right. \\ &\quad \left. + (\boldsymbol{e}_k \boldsymbol{e}_k^T - \boldsymbol{H}_k \boldsymbol{P}_k^- \boldsymbol{H}_k^T) \right] \\ &= \left(1 - \frac{1}{k} \right) \boldsymbol{R}_{k-1} + \frac{1}{k} (\boldsymbol{e}_k \boldsymbol{e}_k^T - \boldsymbol{H}_k \boldsymbol{P}_k^- \boldsymbol{H}_k^T). \end{aligned} \quad (33)$$

In order to improve the adaptive ability of Eq. (33), it is rewritten as

$$\boldsymbol{R}_k = (1 - \eta_k) \boldsymbol{R}_{k-1} + \eta_k (\boldsymbol{e}_k \boldsymbol{e}_k^T - \boldsymbol{H}_k \boldsymbol{P}_k^- \boldsymbol{H}_k^T), \quad (34)$$

$$\eta_k = \frac{\eta_{k-1}}{\eta_{k-1} + b}, \quad (35)$$

where $\eta_0 = 1$, and $0 < b < 1$ is called the fading factor, which is usually $b = 0.9 \sim 0.999$.

In order to improve the reliability of \boldsymbol{R}_k in the adaptive process, sequential filtering is adopted and the upper boundary limit $R_{\max}^{(i)}$ and lower boundary limit $R_{\min}^{(i)}$ are set on each diagonal component of \boldsymbol{R}_k , which is forced to keep it in a reasonable range all the time. \boldsymbol{R}_k is a diagonal matrix, and the superscript (i) represents the i th element of the matrix. Equation (34) can be rewritten as

$$R_k^{(i)} = \begin{cases} (1 - \eta_k) R_{k-1}^{(i)} + \eta_k R_{\min}^{(i)} & p_k^{(i)} < R_{\min}^{(i)} \\ R_{\max}^{(i)} & p_k^{(i)} > R_{\max}^{(i)} \\ (1 - \eta_k) R_{k-1}^{(i)} + \eta_k p_k^{(i)} & \text{others} \end{cases}, \quad (36)$$

$$p_k^{(i)} = \boldsymbol{e}_k^{(i)} \boldsymbol{e}_k^{(i)T} - \boldsymbol{H}_k^{(i)} \boldsymbol{P}_k^{-{(i)}} \boldsymbol{H}_k^{(i)T}. \quad (37)$$

In order to improve the accuracy and robustness of the calibration method, integral in the time interval of interest on both sides of Eq. (18), it can be obtained that

$$\int_0^k \mathbf{C}_n^b \mathbf{v}^n(t) dt = \int_0^k (1 + \delta K) \mathbf{C}_m^b \mathbf{v}_{LDV}^m(t) dt. \quad (38)$$

Based on the fundamental of the inertial navigation, the update equation of position in the n frame is

$$\dot{\mathbf{P}}^n = \mathbf{R}_c \mathbf{v}^n, \quad (39)$$

where

$$\mathbf{R}_c = \begin{bmatrix} 0 & 1/(R_M + b) & 0 \\ \sec L/(R_N + b) & 0 & 0 \\ 0 & 0 & 1 \end{bmatrix}. \quad (40)$$

Substituting Eq. (39) into Eq. (38), we can get

$$\int_0^k \mathbf{C}_n^b \mathbf{R}_c^{-1} \dot{\mathbf{P}}^n dt = (1 + \delta K) \mathbf{C}_m^b \int_0^k \mathbf{v}_{LDV}^m(t) dt. \quad (41)$$

The discretization form of Eq. (41) can be expressed as

$$\sum_{i=0}^{M-1} \mathbf{C}_n^b(k_{i+1}) \mathbf{R}_c^{-1}(k_{i+1}) [\mathbf{P}^n(k_{i+1}) - \mathbf{P}^n(k_i)] = (1 + \delta K) \mathbf{C}_m^b \sum_{i=0}^{M-1} [\mathbf{v}_{LDV}^m(k_{i+1}) + \mathbf{v}_{LDV}^m(k_i)] \frac{T}{2}. \quad (42)$$

Similar to Eq. (19), the scale factor error is calculated by Eq. (42) as

$$\delta K_P = \frac{\left\| \sum_{i=0}^{M-1} \mathbf{C}_n^b(k_{i+1}) \mathbf{R}_c^{-1}(k_{i+1}) [\mathbf{P}^n(k_{i+1}) - \mathbf{P}^n(k_i)] \right\|}{\left\| \sum_{i=0}^{M-1} [\mathbf{v}_{LDV}^m(k_{i+1}) + \mathbf{v}_{LDV}^m(k_i)] \frac{T}{2} \right\|} - 1. \quad (43)$$

The observation vector equation based on position observation can be given by

$$\boldsymbol{\beta}_P(k) = \mathbf{C}_m^b \boldsymbol{\alpha}_P(k), \quad (44)$$

where

$$\begin{cases} \boldsymbol{\alpha}_P(k) = (1 + \delta K) \sum_{i=0}^{M-1} [\mathbf{v}_{LDV}^m(k_{i+1}) + \mathbf{v}_{LDV}^m(k_i)] \frac{T}{2} \\ \boldsymbol{\beta}_P(k) = \sum_{i=0}^{M-1} \mathbf{C}_n^b(k_{i+1}) \mathbf{R}_c^{-1}(k_{i+1}) [\mathbf{P}^n(k_{i+1}) - \mathbf{P}^n(k_i)]. \end{cases} \quad (45)$$

5. VEHICLE-MOUNTED FIELD TEST

To verify the performance of the proposed calibration method based on position observation, two vehicle tests were carried out in Changsha. Figure 2 shows the test equipment, which included the self-developed inertial measurement unit (IMU), dual-antenna GNSS receiver, navigation computer, and self-made LDV. The IMU consists of three ring laser gyroscopes with bias instability of $0.008^\circ/h$ and random walk of $0.003^\circ/\sqrt{h}$, and three quartz accelerometers with bias instability of $50 \mu g$ and random walk of $50 \mu g/\sqrt{h}$. The velocity measurement error of the LDV is $0.1\% (1\sigma)$. The GNSS can only provide location information, where the horizontal positioning accuracy

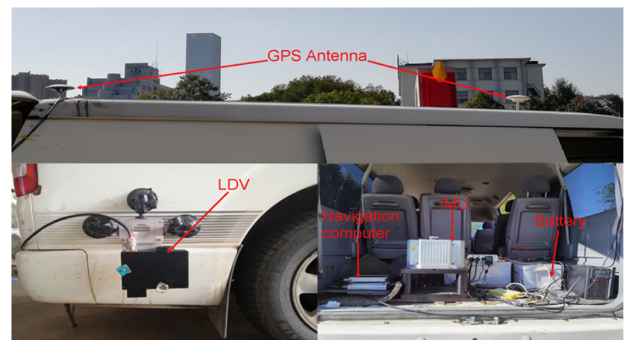


Fig. 2. Installation diagram of the experimental system.

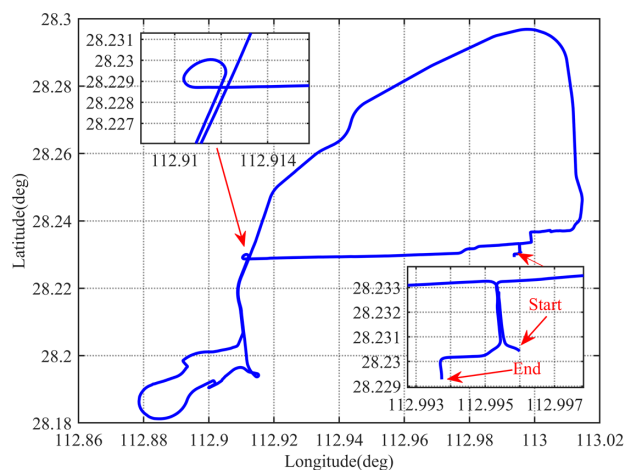


Fig. 3. Trajectory of the vehicle in the first vehicle test.

and the altitude accuracy are within 0.1 m. The GNSS data output frequency is 10 Hz, whereas the data output frequency of the IMU and LDV is 100 Hz. The vehicle remains stationary at the start point for about 13 min before moving and the static attitude alignment is performed to obtain the accurate initial attitude.

The following schemes are designed for comparison to evaluate the calibration performance of the proposed method based on position observation.

Scheme 1. The calibration method proposed in this paper, which based on velocity observation.

Scheme 2. The calibration method proposed in this paper, which based on position observation.

Scheme 3. The calibration scheme based on the Kalman filter.

The movement trajectory of the first vehicle test is shown in Fig. 3. The output velocity of the LDV and the velocity obtained by the GNSS/SINS integration system with the Kalman filter are shown in Fig. 4. The scale factor error curve is shown in Fig. 5, where Scheme 1 is marked by the red line, Scheme 2 is marked by the blue line, and Scheme 3 is marked by the green line. As can be seen from Fig. 5, Scheme 2 and Scheme 3 can effectively estimate the scale factor error. However, Scheme 1 fluctuates sharply, because Scheme 1 only uses the velocity information, it will not be able to effectively resist the interference of measurement error and velocity noise and outliers.

The pitch misalignment angle and heading misalignment angle of the LDV are shown in Figs. 6 and 7. As can be seen

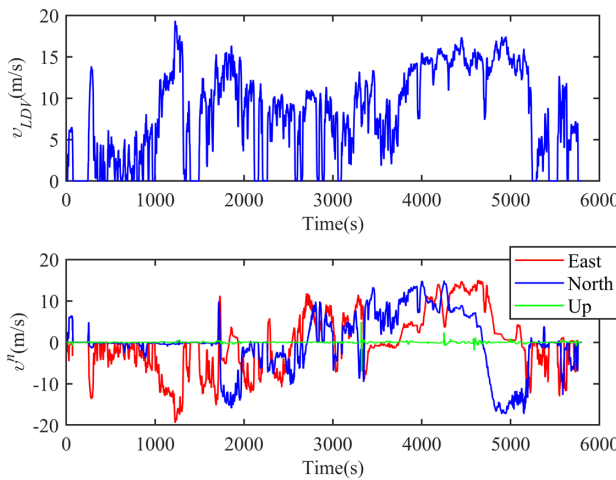


Fig. 4. LDV and GNSS/SINS integration system velocity output curve in the first vehicle test.

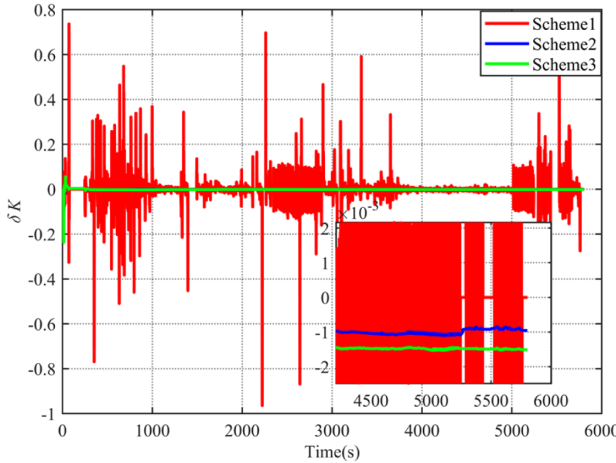


Fig. 5. Curve of the scale factor error in the first vehicle test.

in Figs. 6 and 7, the convergence of the pitch misalignment angle and heading misalignment angle of the LDV in Scheme 2 is smoother than other schemes, because Scheme 2 based on position observation can effectively weaken the influence of LDV velocity noise and GNSS outliers. The convergence speed of the heading misalignment angle of the LDV in Scheme 3 is the fastest in all schemes, but its stability and the convergence speed and stability of the pitch misalignment angle of the LDV are worse than Scheme 2. The calibration effect of Scheme 1 is the worst among all schemes, where the convergence speed of the pitch misalignment angle and heading misalignment angle

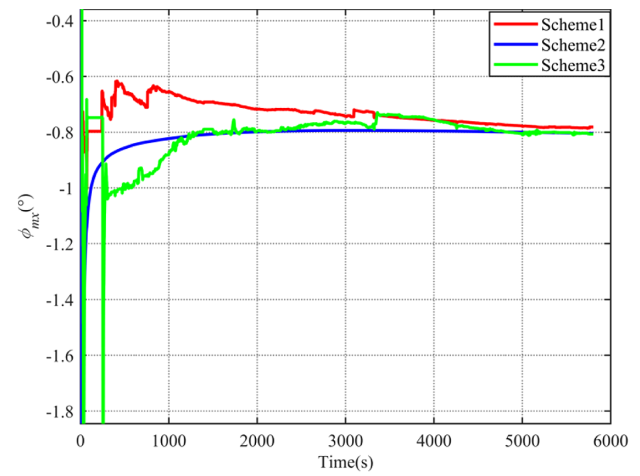


Fig. 6. Curve of the pitch misalignment angle in the first vehicle test.

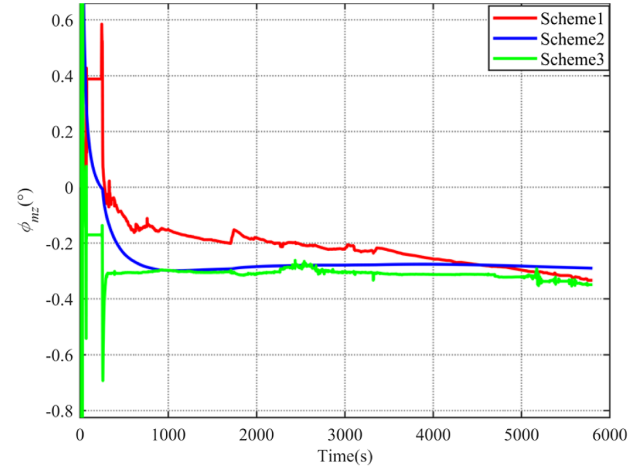


Fig. 7. Curve of the heading misalignment angle in the first vehicle test.

of the LDV is the slowest in all schemes, and the stability is not satisfactory, because it is hard to resist noise based on velocity observation. In order to further analyze the calibration performance of each scheme, the dead reckoning of the LDV/SINS integrated system is carried out by using the calibration results of each scheme at different time points, and the position error is shown in Table 1.

From the maximum position error in dead reckoning caused by the calibration results of different schemes at different time points in Table 1, it can be seen that the horizontal error and

Table 1. Positioning Error of the LDV/SINS Dead Reckoning

Time(s)		0s	600s	1000s	2000s	3000s	4000s	5000s	End
Scheme 1	Horizontal Error (m)	71.55	75.77	77.43	115.22	243.71	53.23	30.83	20.53
	Vertical Error (m)	683.15	130.77	144.20	93.75	73.92	60.97	43.94	42.41
Scheme 2	Horizontal Error (m)	71.55	15.53	15.07	14.94	14.91	14.87	14.92	14.91
	Vertical Error (m)	683.15	11.73	8.761	28.41	32.59	30.98	27.29	23.51
Scheme 3	Horizontal Error (m)	71.55	19.99	19.71	15.17	15.07	15.20	16.17	19.31
	Vertical Error (m)	683.15	128.88	39.71	31.64	53.61	64.56	20.81	23.06

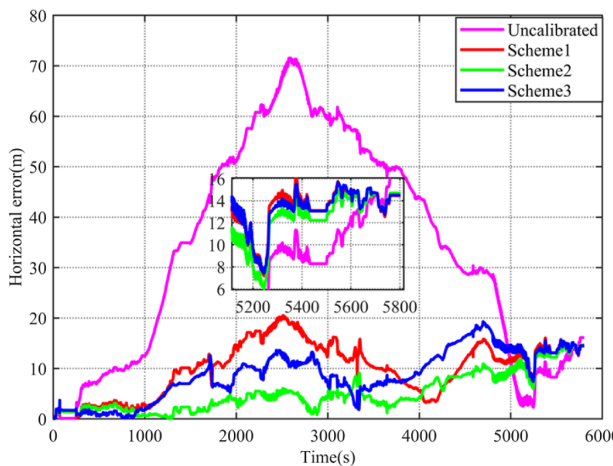


Fig. 8. Horizontal position error of the LDV/SINS integrated navigation system in the first vehicle test.

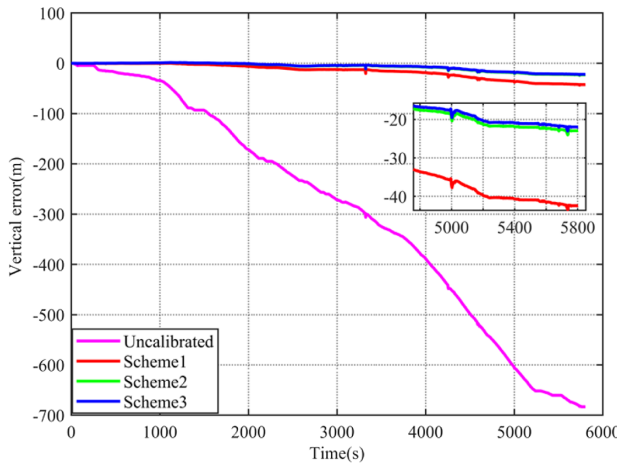


Fig. 9. Vertical position error of the LDV/SINS integrated navigation system in the first vehicle test.

vertical error of Scheme 2 are the most satisfactory, and Scheme 3 has a smaller horizontal error, but a long calibration time is needed to obtain a satisfactory vertical error. Scheme 1 has the worst horizontal error and vertical error. The results of position errors in Table 1 are completely consistent with the changing trend of the correlation curves in Figs. 5–7. The horizontal and vertical errors in the dead reckoning of the LDV/SINS integrated system using the final calibration results are shown in Figs. 8 and 9. In the test with a total mileage of 47.49 km, the maximum horizontal error and maximum vertical error of the LDV/SINS integrated system calibrated by Scheme 2 are 14.91 m and 23.51 m, respectively, and the horizontal position accuracy is less than 0.0314% of the mileage.

In order to further verify the robustness of the calibration method proposed in this paper, the second vehicle test was carried out. The movement trajectory is shown in Fig. 10, and the output velocity of the LDV and the velocity obtained by the GNSS/SINS integration system with the Kalman filter are shown in Fig. 11. It can be found that there are outliers contained in the velocity outputs of the GNSS/SINS integration system, which is because the position information provided

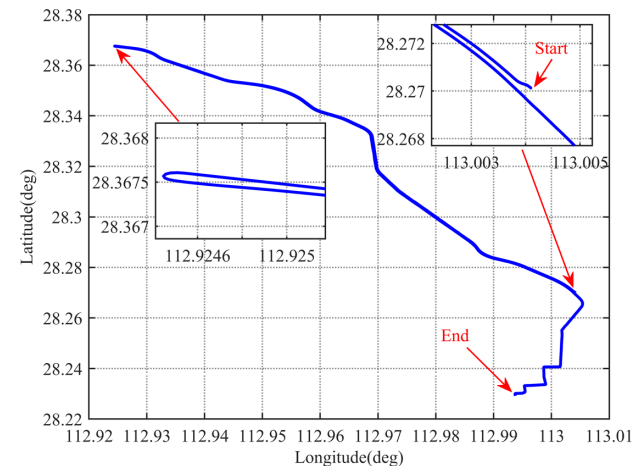


Fig. 10. Trajectory of the vehicle in the second vehicle test.

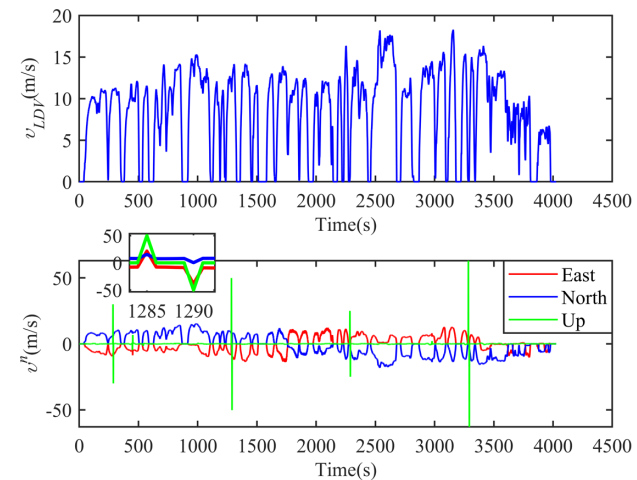


Fig. 11. LDV and GNSS/SINS integration system velocity output curve in the second vehicle test.

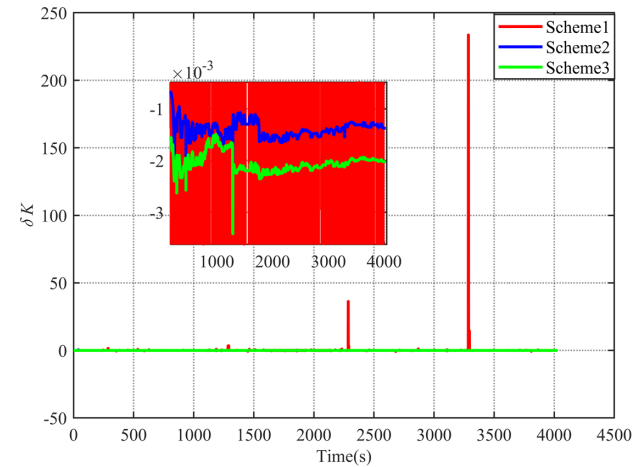


Fig. 12. Curve of the scale factor error in the second vehicle test.

by the GNSS contains outliers. The scale factor error, pitch misalignment angle, and heading misalignment angle of the LDV are shown in Figs. 12–14.

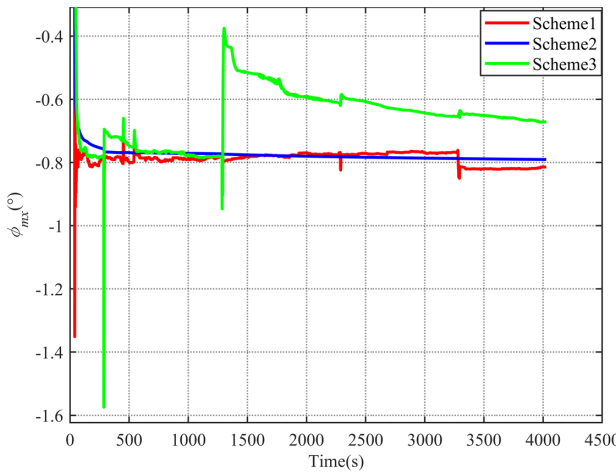


Fig. 13. Curve of the pitch misalignment angle in the second vehicle test.

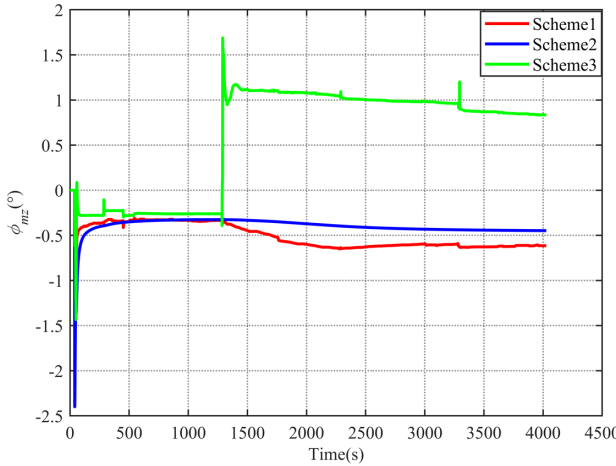


Fig. 14. Curve of the heading misalignment angle in the second vehicle test.

From Figs. 12–14, we can see that the superiority of Scheme 2 is obvious compared with the other schemes. The calibration results of Scheme 2 show that the calibration method based on position observation can enhance the robustness of the calibration process of the LDV, because the magnitude of the position trajectory is much larger than the corresponding magnitude of the outliers and noise. In contrast, in Fig. 11, the magnitude of the velocity is even much smaller than the corresponding magnitude of the outliers. This is one of the reasons why the calibration method based on position observation is better than the calibration method based on velocity information. The horizontal and vertical errors in the dead reckoning of the LDV/SINS integrated system using the final calibration results of the second tests are shown in Figs. 15 and 16. As shown in Figs. 15 and 16, in the test with a total mileage of 33.45 km, the maximum horizontal error and maximum vertical error of the LDV/SINS integrated system calibrated by Scheme 2 are 34.57 m (0.1033% of the travel mileage) and 11.36 m, respectively, which are much smaller than those of the other schemes.

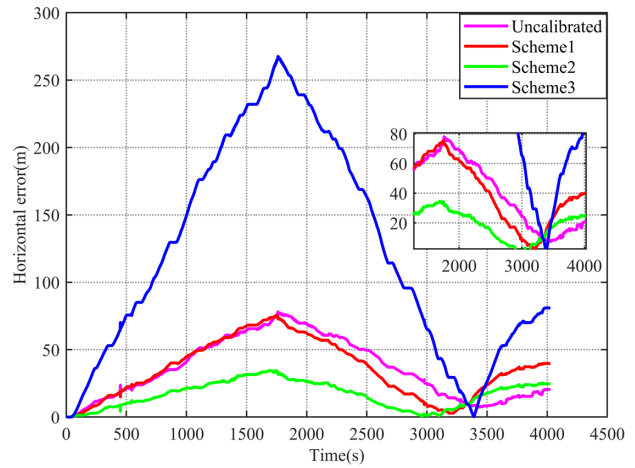


Fig. 15. Horizontal position error of the LDV/SINS integrated navigation system in the second vehicle test.

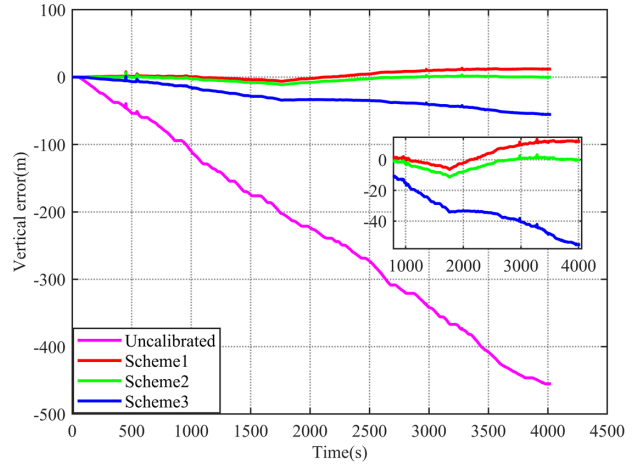


Fig. 16. Vertical position error of the LDV/SINS integrated navigation system in the second vehicle test.

6. CONCLUSION

In this paper, a robust calibration method aided GNSS is proposed, which is based on position observation. Different from the current popular calibration method, the proposed method obtains the attitude and velocity information of the GNSS/SINS integrated navigation system by the adaptive Kalman filter, and uses the velocity outputs of the LDV and position outputs of the GNSS to construct the observation vector. This effectively weakens the interference of LDV velocity noise and GNSS outliers, and determines the scale factor error of the LDV by the ratio of the modules of two observation vectors, while the misalignment angle of the LDV is determined by solving observation vectors by Davenport's q-method. In addition, the calibration method based on velocity observation is introduced in this paper, and together with the mainstream Kalman filter calibration method as the comparison method of the calibration method proposed in this paper. Two vehicle tests verify the robustness and accuracy of the proposed calibration method. The first vehicle test shows that the proposed method can smooth the calibration results and has higher calibration accuracy than other methods under the condition of no outlier

interference, where the horizontal position error of dead reckoning of the LDV/SINS integrated system is less than 0.0314% of the mileage. The second vehicle test shows that the antijamming ability of this method is obviously better than that of other methods under the interference of outliers, where the horizontal position accuracy of dead reckoning of the LDV/SINS integrated system is less than 0.1033% of the mileage.

Funding. Major Basic Autonomous Research Project of the College of Advanced Interdisciplinary Studies, National University of Defense Technology (ZDJC19-12).

Disclosures. The authors declare no conflicts of interest.

Data Availability. Data underlying the results presented in this paper are not publicly available at this time but may be obtained from the authors upon reasonable request.

REFERENCES

1. D. H. Titterton, J. L. Weston, and J. L. Weston, and The Institution of Electrical Engineers, *Strapdown Inertial Navigation Technology*, IEE Radar, Sonar, Navigation and Avionics Series (Institution of Electrical Engineers, Peter Peregrinus Limited, 1997).
2. P. D. Groves, *Principles of GNSS, Inertial, and Multisensor Integrated Navigation Systems*, GNSS Technology and Applications Series (Artech House, 2008).
3. Y. Wu, "Velocity/position integration formula part II: application to strapdown inertial navigation computation," *IEEE Trans. Aerosp. Electron. Syst.* **49**, 1024–1034 (2013).
4. S. Rezaei and R. Sengupta, "Kalman filter-based integration of DGPS and vehicle sensors for localization," *IEEE Trans. Control Syst. Technol.* **15**, 1080–1088 (2007).
5. S. B. Kim, J. C. Bazin, H. K. Lee, K. H. Choi, and S. Y. Park, "Ground vehicle navigation in harsh urban conditions by integrating inertial navigation system, global positioning system, odometer and vision data," *IET Radar Sonar Navig.* **5**, 814–823 (2011).
6. A. El-Mowafy and N. Kubo, "Integrity monitoring for positioning of intelligent transport systems using integrated RTK-GNSS, IMU and vehicle odometer," *IET Intell. Transp. Syst.* **12**, 901–908 (2018).
7. L. Chang, Y. Li, and B. Xue, "Initial alignment for a Doppler velocity log-aided strapdown inertial navigation system with limited information," *IEEE/ASME Trans. Mechatronics* **22**, 329–338 (2017).
8. P. Liu, B. Wang, Z. Deng, and M. Fu, "INS/DVL/PS tightly coupled underwater navigation method with limited DVL measurements," *IEEE Sens. J.* **18**, 2994–3002 (2018).
9. B. Liang and L. Pengz, "On integrated navigation for vehicle dead reckoning," *Comput. Meas. Control* **18**, 2379–2384 (2010).
10. Z. Jian and L. Xingwu, "Research on laser Doppler velocimeter for vehicle self-contained inertial navigation system," *Opt. Laser Technol.* **42**, 477–483 (2010).
11. J. Zhou, "Research on multipoint layer-type laser Doppler self-velocimeter," *Opt. Eng.* **49**, 44301 (2010).
12. J. Zhou, X. Nie, and J. Lin, "A novel laser Doppler velocimeter and its integrated navigation system with strapdown inertial navigation," *Opt. Laser Technol.* **64**, 319–323 (2014).
13. X. Nie and J. Zhou, "Pitch independent vehicle-based laser Doppler velocimeter," *Opt. Lasers Eng.* **131**, 106072 (2020).
14. Q. Wang, C. Gao, J. Zhou, G. Wei, X. Nie, and X. Long, "Two-dimensional laser Doppler velocimeter and its integrated navigation with a strapdown inertial navigation system," *Appl. Opt.* **57**, 3334–3339 (2018).
15. R. Huang, Q. Wang, X. Nie, and J. Zhou, "One-dimensional reference-beam LDV for accurate altitude estimation in a land vehicle," *Appl. Opt.* **59**, 10667–10672 (2020).
16. P. M. Lee, B. H. Jun, K. Kim, J. Lee, T. Aoki, and T. Hyakudome, "Simulation of an inertial acoustic navigation system with range aiding for an autonomous underwater vehicle," *IEEE J. Ocean. Eng.* **32**, 327–345 (2007).
17. L. Li, H. Sun, S. Yang, X. Ding, J. Wang, J. Jiang, X. Pu, C. Ren, N. Hu, and Y. Guo, "Online calibration and compensation of total odometer error in an integrated system," *Measurement* **123**, 69–79 (2018).
18. B. Xu, L. Wang, S. Li, and J. Zhang, "A novel calibration method of SINS/DVL integration navigation system based on quaternion," *IEEE Sens. J.* **20**, 9567–9580 (2020).
19. R. Pollard and J. Read, "A method for calibrating shipmounted acoustic Doppler profilers and the limitations of gyro compasses," *J. Atmos. Ocean. Technol.* **6**, 859–865 (1989).
20. G. Troni and L. L. Whitcomb, "Advances in in situ alignment calibration of Doppler and high/low-end attitude sensors for underwater vehicle navigation: theory and experimental evaluation," *J. Field Robot.* **32**, 655–674 (2015).
21. W. Li, L. Zhang, F. Sun, L. Yang, M. Chen, and Y. Li, "Alignment calibration of IMU and Doppler sensors for precision INS/DVL integrated navigation," *Optik* **126**, 3872–3876 (2015).
22. D. Wang, X. Xu, Y. Yang, and T. Zhang, "A quasi-Newton quaternions calibration method for DVL error aided GNSS," *IEEE Trans. Veh. Technol.* **70**, 2465–2477 (2021).
23. Q. Wang, X. Nie, C. Gao, J. Zhou, G. Wei, and X. Long, "Calibration of a three-dimensional laser Doppler velocimeter in a land integrated navigation system," *Appl. Opt.* **57**, 8566–8572 (2018).
24. Y. Zhu, X. Wang, J. Zheng, H. Xiong, and Y. Zhao, "Using GPS time-differenced carrier phase observations to calibrate LDV/INS integrated navigation systems," *IEEE Sens. J.* **20**, 405–414 (2020).
25. M. Wu, Y. Wu, X. Hu, and D. Hu, "Optimization-based alignment for inertial navigation systems: theory and algorithm," *Aerospace Sci. Technol.* **15**, 1–17 (2011).
26. J. R. Wertz, *Spacecraft Attitude Determination and Control, Astrophysics and Space Science Library* (Springer, 2012).
27. C. Gao, Q. Wang, G. Wei, and X. Long, "A highly accurate calibration method for terrestrial laser Doppler velocimeter," *IEEE Trans. Instrum. Meas.* **66**, 1994–2003 (2017).
28. M. Liu, G. Li, Y. Gao, S. Li, and L. Guan, "Velocity-aided in-motion alignment for SINS based on pseudo-Earth frame," *J. Navig.* **71**, 221–240 (2018).
29. K. Tang, J. Wang, W. Li, and W. Wu, "A novel INS and Doppler sensors calibration method for long range underwater vehicle navigation," *Sensors* **13**, 14583–14600 (2013).
30. X. Pan and Y. Wu, "Underwater Doppler navigation with self-calibration," *J. Navig.* **69**, 295–312 (2016).
31. J. L. Crassidis, F. L. Markley, and Y. Cheng, "Survey of nonlinear attitude estimation methods," *J. Guid. Control. Dyn.* **30**, 12–28 (2007).
32. G. Chang, T. Xu, and Q. Wang, "Error analysis of Davenport's q method," *Automatica* **75**, 217–220 (2017).
33. M. D. Shuster and S. D. Oh, "Three-axis attitude determination from vector observations," *J. Guid. Control* **4**, 70–77 (1981).